Mathematical, Thermodynamical, and Experimental Necessity for Coarse Graining Empirical Densities and Currents in Continuous Space

Cai Dieball and Aljaž Godec*
Mathematical bioPhysics Group, Max Planck Institute for Multidisciplinary Sciences, Am Faßberg 11, 37077 Göttingen

(Received 24 May 2021; revised 19 July 2022; accepted 28 July 2022; published 29 September 2022)

We present general results on fluctuations and spatial correlations of the coarse-grained empirical density and current of Markovian diffusion in equilibrium or nonequilibrium steady states on all timescales. We unravel a deep connection between current fluctuations and generalized time-reversal symmetry, providing new insight into time-averaged observables. We highlight the essential role of coarse graining in space from mathematical, thermodynamical, and experimental points of view. Spatial coarse graining is required to uncover salient features of currents that break detailed balance, and a thermodynamically "optimal" coarse graining ensures the most precise inference of dissipation. Defined without coarse graining, the fluctuations of empirical density and current are proven to diverge on all timescales in dimensions higher than one, which has far-reaching consequences for the central-limit regime in continuous space. We apply the results to examples of irreversible diffusion. Our findings provide new intuition about time-averaged observables and allow for a more efficient analysis of single-molecule experiments.

DOI: 10.1103/PhysRevLett.129.140601

Single-molecule experiments [1–5] probe equilibrium and nonequilibrium (i.e., detailed balance violating) processes during relaxation [6–12] or in steady states [13–21] on the level of individual trajectories. These are typically analyzed by averaging along individual realizations yielding random quantities with nontrivial statistics [22,23]. Time-averaged observables, in particular generalized currents, are central to stochastic thermodynamics [16,24–28]. Such time-average statistical mechanics focuses on functionals of a trajectory $(\mathbf{x}_\tau)_{0\le\tau\le t}$, in particular the empirical density (or occupation time [29–37]) $\overline{\rho_{\mathbf{x}}}(t)$ and current $\overline{\mathbf{J}_{\mathbf{x}}}(t)$ at a point $\mathbf{x}$. Necessary in the analysis of laboratory [1,38] or computer [39] experiments with a finite spatial resolution, and useful for smoothing data *a posteriori* to improve statistics, the density and current should be defined as spatial averages over a window $U^h_{\mathbf{x}}(\mathbf{x}')$ at $\mathbf{x}$ with coarse-graining scale h

$$\overline{\rho^U_{\mathbf{x}}}(t) \equiv \frac{1}{t}\int_0^t U^h_{\mathbf{x}}(\mathbf{x}_\tau)d\tau, \qquad \overline{\mathbf{J}^U_{\mathbf{x}}}(t) \equiv \frac{1}{t}\int_{\tau=0}^{\tau=t} U^h_{\mathbf{x}}(\mathbf{x}_\tau)\circ d\mathbf{x}_\tau, \tag{1}$$

where $\circ d\mathbf{x}_\tau$ denotes the Stratonovich integral. These observables are illustrated in terms of sojourns of the window in Figs. 1(a) and 1(b). Choosing the window $U^h_{\mathbf{x}}$ as a bin, the density and current observables appear as histograms along single trajectories over occupations of or displacements in the bin that fluctuate between different realizations [see Figs. 1(c)–1(e) and companion extended paper [40]]. Aside from coarse graining, the integration over $U^h_{\mathbf{x}}(\mathbf{x}')$ may also represent a pathwise thermodynamic potential, e.g., heat dissipation (the force integrated along a stochastic path $\int_{\tau=0}^{\tau=t}\mathbf{F}(\mathbf{x}_\tau)\cdot\circ d\mathbf{x}_\tau$ [24]) or generalized currents [18,27,28,41]. Normalized windows, i.e., $\int U^h_{\mathbf{x}}(\mathbf{z})d\mathbf{z} = 1$, yield $\overline{\rho^U_{\mathbf{x}}}(t)$ and $\overline{\mathbf{J}^U_{\mathbf{x}}}(t)$ that are estimators of the probability density and current density, respectively. The usually defined empirical density $\overline{\rho_{\mathbf{x}}}(t)$ and current $\overline{\mathbf{J}_{\mathbf{x}}}(t)$ [14,42–50] correspond to no coarse graining, i.e., $U^{h=0}_{\mathbf{x}}(\mathbf{z})$ being Dirac's delta function $\delta(\mathbf{x}-\mathbf{z})$.

Reliably inferring from noisy trajectories whether a system obeys detailed balance, notwithstanding recent progress [1,2,38,39,51–55], remains challenging. *Quantifying* violations of detailed balance is a daunting task. One can quantify broken detailed balance through violations of the fluctuation dissipation theorem [19,56,57], which requires perturbing the system from the steady state. One can also check for a symmetry breaking of forward and backward transition-path times [53,54], measure the entropy production [51,55,58,59], or infer steady-state currents [see arrows in Fig. 1(c)] directly [1,38], all of which require substantial statistics. However, single-molecule experiments often cannot reach ergodic times, have a finite resolution, and only allow for a limited number of repetitions. This leads to uncertainties in estimates of observables such as steady-state

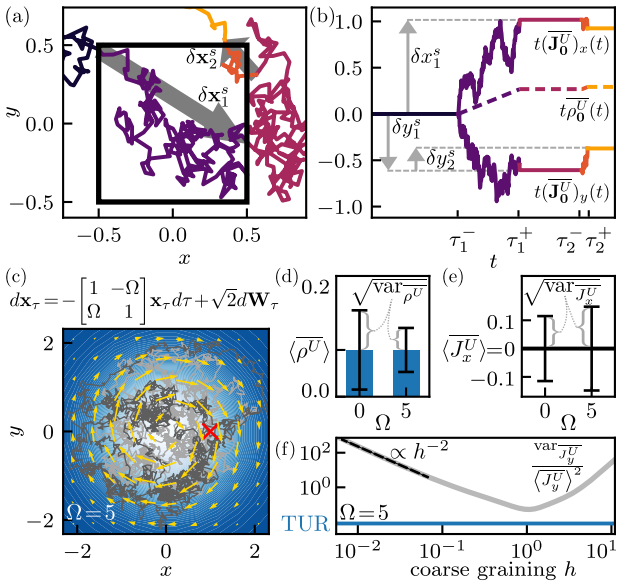

FIG. 1. (a) Diffusive trajectory traversing an observation window $U_\mathbf{0}^h(x,y) = 1$ if $|x|, |y| \le 1/2$ and $U_\mathbf{0}^h(x,y) = 0$ otherwise, with time running from dark to bright. Arrows denote contributions $\delta\mathbf{x}_i^s = (\delta x_i^s, \delta y_i^s)$ of the two sojourns in $U_\mathbf{0}^h$ between times τ_i^- and τ_i^+ (see Eq. (A1) in Appendix A). (b) Corresponding $t\overline{\rho_\mathbf{0}^U}(t)$ and components of $t\overline{\mathbf{J}_\mathbf{0}^U}(t)$ from Eq. (1) as functions of t. (c) Two trajectories $(\mathbf{x}_\tau)$ (gray lines) of length $t = 5$ in confined rotational flow with $\Omega = 5$ (arrows depict the steady-state current $\mathbf{j}_\mathrm{s}$). The red cross is the reference point $\mathbf{x}_R = (1, 0)$ considered in (d)–(f). Coarse-grained density (d) and x current (e) for a Gaussian window $U_{\mathbf{x}_R}^h$ with $h = 0.3$. Fluctuations of $\overline{\rho_\mathbf{x}^U}$ and $\overline{J_{x,y}^U} \equiv (\overline{\mathbf{J}_{\mathbf{x}_R}^U})_{x,y}$ encode violations of detailed balance even where $\overline{J_x^U}$ vanishes. (f) Squared relative error of $\overline{J_y^U}$ for $U_{\mathbf{x}_R}^h$ as a function of h (gray) bounded by the thermodynamic uncertainty relation (TUR; blue). A variance diverging as h^{-2} (dashed) as $h \to 0$ and vanishing mean for $h \gg 1$ allow for intermediate h optimizing the TUR-bound and thus the inferred dissipation.

currents [see Figs. 1(d)–1(f). Notably, fluctuations of $\overline{\rho_\mathbf{x}^U}$ and $\overline{\mathbf{J}_\mathbf{x}^U}$ encode information about violations of detailed balance [even where the mean current or its components locally vanish; see Figs. 1(d) and 1(e)], which *a priori* is hard to interpret.

Current fluctuations have a noise floor—they are bounded from below by the "thermodynamic uncertainty relation" [16–18] which in turn allows for bounding dissipation in a system from below by current fluctuations [26,60–62]. As we show in Fig. 1(f) (see Ref. [40] for a multiwell potential) the precision of inferring dissipation typically depends nonmonotonically on the coarse-graining scale h—given a system, a point $\mathbf{x}$, and trajectory length t there exists a thermodynamically "optimal" coarse graining due to a diverging variance for $h \to 0$ and vanishing mean for large h. Moreover, $\overline{\rho_\mathbf{x}}$ and $\overline{\mathbf{J}_\mathbf{x}}$ without coarse graining turn out to be ill defined.

In systems and on timescales where dynamics is reasonably described by a Markov jump process on a small state space, current fluctuations are well understood [15,16,46,63–77]. However, dynamics typically evolves in continuous space, and a continuous dynamics observed on a discrete space is *not* Markovian [78,79] (see Ref. [80] for a quantitative confirmation). An accurate Markov jump description may require too many states to be practical, and is known to fail when considering functionals as in Eq. (1) [79]. We therefore focus on continuous space, where, with exceptions [14,18,86,87], insight is limited to hydrodynamic scales [66,68,88] and large deviations [42–50]. A comprehensive understanding of fluctuations and spatial correlations of density and current in continuous space remains elusive, and the interpretation of the typical definition without coarse graining in dimensions $d \ge 2$ apparently requires a revision, see below.

Here, we provide general results on the empirical density and current in overdamped diffusive steady-state systems, revealing a mathematical, thermodynamical, and experimental necessity for spatial coarse graining. When defined in a point, fluctuations are proven to diverge in spatial dimensions above one, contradicting existing central-limit statements. We explain why a systematic variation of the coarse-graining scale provides deeper insight about the underlying dynamics and allows for improved inference of the system's thermodynamics. Exploiting a generalized time-reversal symmetry we provide intuition about fluctuating currents along individual trajectories. Nonvanishing density-current correlations are shown to unravel violations of detailed balance from short measurements. Our results allow for a more consistent and efficient analysis of experiments, and provide new insight into nonequilibrium steady states and their thermodynamics.

Setup.—We consider time-homogeneous overdamped Langevin dynamics [81,89] in d-dimensional space evolving according to the stochastic differential equation $d\mathbf{x}_\tau = \mathbf{F}(\mathbf{x}_\tau)d\tau + \boldsymbol{\sigma} d\mathbf{W}_\tau$, where $d\mathbf{W}_\tau$ is the increment of a d-dimensional Wiener processes (i.e., white noise) with covariance $\langle dW_{\tau,i} dW_{\tau',j}\rangle = \delta(\tau - \tau')\delta_{ij} d\tau d\tau'$. The Fokker-Planck equation for the conditional probability density with initial condition $G(\mathbf{x},0|\mathbf{y}) = \delta(\mathbf{x}-\mathbf{y})$ reads $(\partial_t + \nabla_\mathbf{x} \cdot \hat{\mathbf{j}}_\mathbf{x}) \times G(\mathbf{x}, t|\mathbf{y}) = 0$ with current operator $\hat{\mathbf{j}}_\mathbf{x} \equiv \mathbf{F}(\mathbf{x}) - \mathbf{D}\nabla_\mathbf{x}$, where $\mathbf{D} \equiv \boldsymbol{\sigma}\boldsymbol{\sigma}^T/2$ is the positive definite diffusion matrix. All results directly generalize to multiplicative noise (see Ref. [40]). The drift $\mathbf{F}(\mathbf{x})$ is assumed to be sufficiently smooth and confining to ensure the existence of a steady-state density $G(\mathbf{x}, t \to \infty|\mathbf{y}) = p_\mathrm{s}(\mathbf{x})$ and, if detailed balance is violated, a steady-state current $\mathbf{j}_\mathrm{s}(\mathbf{x}) \equiv \hat{\mathbf{j}}_\mathbf{x} p_\mathrm{s}(\mathbf{x}) \neq 0$ [81,89].

Correlations and fluctuations from paths.—To investigate the nontrivial statistics of the observables in Eq. (1) we now outline the derivation detailed in [40] of results for mean values, correlations, and fluctuations assuming steady-state initial conditions. Let $\langle\cdot\rangle_s$ denote the average over all paths $(\mathbf{x}_\tau)$ evolving from p_s. The mean values $\langle\overline{\rho_\mathbf{x}^U}(t)\rangle_s = \int d\mathbf{z} U_\mathbf{x}^h(\mathbf{z}) p_\mathrm{s}(\mathbf{z})$ and $\langle\overline{\mathbf{J}_\mathbf{x}^U}(t)\rangle_\mathrm{s} = \int d\mathbf{z} U_\mathbf{x}^h(\mathbf{z}) \mathbf{j}_\mathrm{s}(\mathbf{z})$ [40] are time-independent estimators of the

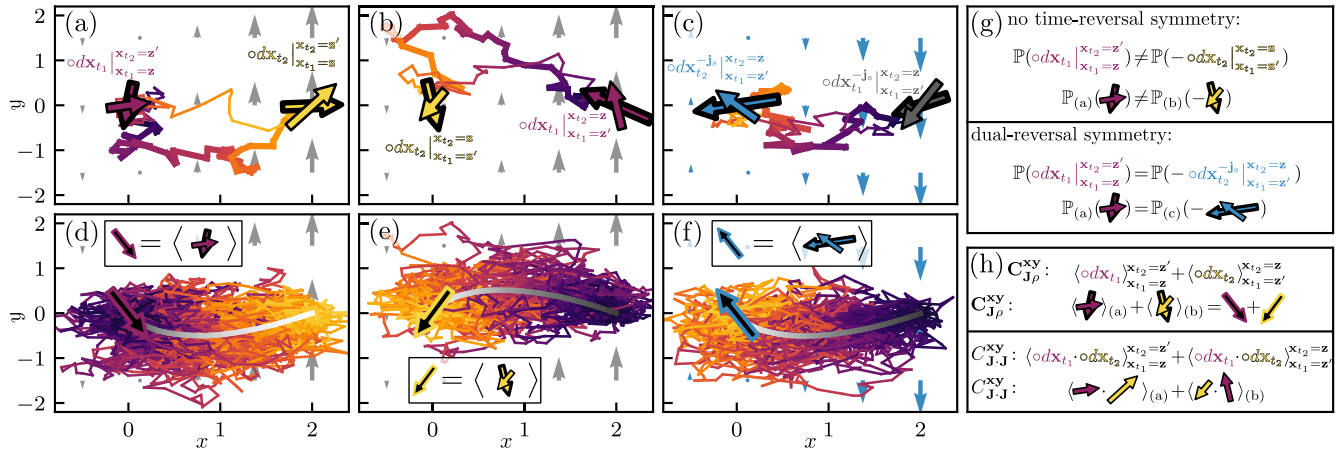

FIG. 2. (a) Two sample trajectories in a shear flow $\mathbf{F}_{\rm sh}(\mathbf{x})$ (gray arrows) with Stratonovich displacements $\circ d\mathbf{x}_t$ in the initial $\mathbf{x}_{t_1} = \mathbf{z}$ and final point $\mathbf{x}_{t_2} = \mathbf{z}'$ for fixed $t_1 < t_2$ depicted by purple and yellow arrows, respectively. Time is running from dark to bright. (b) Trajectories as in (a) but running from $\mathbf{x}_{t_1} = \mathbf{z}'$ to $\mathbf{x}_{t_2} = \mathbf{z}$. (c) As in (b) but with the inverted shear flow $-\mathbf{F}_{\rm sh}(\mathbf{x}')$ (blue background arrows) and initial and final increments depicted by gray and blue arrows. (d) Ensemble of paths from $\mathbf{x}_{t_1} = \mathbf{z}$ to $\mathbf{x}_{t_2} = \mathbf{z}'$ contributing to $P_{\mathbf{z}}(\mathbf{z}', t_2 - t_1)$. The average initial displacement $\langle \circ d\mathbf{x}_t \rangle_{\mathbf{x}_{t_1}=\mathbf{z}}^{\mathbf{x}_{t_2}=\mathbf{z}'}$ is depicted by the black-purple arrow, and the mean path $\mathbf{z} \to \mathbf{z}'$ in time $t_2 - t_1$ by the gray gradient line. (e) As in (d) but corresponding to (b) instead of (a). (f) As in (e) but with the reversed shear flow as in (c). (g), (h) Since the shear flow breaks time-reversal symmetry, initial-point increments in (a) cannot be obtained by inverting final-point increments in (b). By dual-reversal symmetry initial-point increments follow from inverting the final-point increments in the inverted shear flow in (c), which explains initial point increments $\circ d\mathbf{x}_{t_1}$ in current-density correlations and current (co)variances via the easier and more intuitive final point increments $\circ d\mathbf{x}_{t_2}^{-\mathbf{j}_{\rm s}}$.

steady-state density and current coarse grained over a window $U^h_{\mathbf{x}}$. In contrast to the mean values, covariances display a nontrivial time dependence and therefore contain salient features of the dynamics. We define the two-point steady-state covariance as

$$C^{\mathbf{xy}}_{AB}(t) \equiv \langle A_{\mathbf{x}}(t) B_{\mathbf{y}}(t) \rangle_{\rm s} - \langle A_{\mathbf{x}}(t) \rangle_{\rm s} \langle B_{\mathbf{y}}(t) \rangle_{\rm s}, \qquad (2)$$

where A and B are either $\overline{\rho^U}$ or $\overline{\mathbf{J}^U}$, respectively. We refer to the case $A \neq B$ or $\mathbf{x} \neq \mathbf{y}$ as (linear) correlations and to $A = B$ with $\mathbf{x} = \mathbf{y}$ as fluctuations with the notation $\mathrm{var}^{\mathbf{x}}_A(t) \equiv C^{\mathbf{xx}}_{AA}(t)$. Recall that $\mathrm{var}^{\mathbf{x}}_\rho(t)$ and $\mathrm{var}^{\mathbf{x}}_{\mathbf{J}}(t)$ quantify (experimentally relevant) fluctuations of histograms along single trajectories [see Figs. 1(d) and 1(e)], and $\mathrm{var}^{\mathbf{x}}_{\mathbf{J}}(t)$ is at the heart of the thermodynamic uncertainty relation [see Fig. 1(f)]. Moreover, $C^{\mathbf{xy}}_{\mathbf{J}\rho}(t)$ was recently found to play a vital role in stochastic thermodynamics [28]. All $C^{\mathbf{xy}}_{AB}(t)$ are easily inferred from data, but lack physical understanding. We now give $C^{\mathbf{xy}}_{AB}(t)$ a physical meaning in terms of the statistics of paths pinned at end points $\mathbf{z}$ and $\mathbf{z}'$ (see Fig. 2). Introduce $\langle \cdot \rangle_{\mathbf{x}_{t_1}=\mathbf{z}}^{\mathbf{x}_{t_2}=\mathbf{z}'} \equiv \langle \delta(\mathbf{x}_{t_1} - \mathbf{z}) \delta(\mathbf{x}_{t_2} - \mathbf{z}') \cdot \rangle_{\rm s}$, the Stratonovich increment $\circ d\mathbf{x}_\tau \equiv \mathbf{x}_{\tau + d\tau/2} - \mathbf{x}_{\tau - d\tau/2}$, and the operator

$$\hat{\mathcal{I}}^{t,U}_{\mathbf{xy}}[\cdot] \equiv \frac{1}{t^2} \int_0^t dt_1 \int_{t_1}^t dt_2 \int d\mathbf{z} U^h_{\mathbf{x}}(\mathbf{z}) \int d\mathbf{z}' U^h_{\mathbf{y}}(\mathbf{z}')[\cdot], \qquad (3)$$

where $[\cdot]$ represents functions of t_1, t_2, $\mathbf{z}$, $\mathbf{z}'$, and without loss of generality we choose the convention $\int_{t_1}^t dt_2 \delta(t_2 - t_1) = 1/2$. Upon plugging in mean values $\langle A_{\mathbf{x}} \rangle_{\rm s}$ and $\langle B_{\mathbf{y}} \rangle_s$, the definition (2) becomes [40] $C^{\mathbf{xy}}_{\rho\rho}(t) = \hat{\mathcal{I}}^{t,U}_{\mathbf{xy}}[\Xi^{\mathbf{zz}'}_1 - 2 p_{\rm s}(\mathbf{z}) p_{\rm s}(\mathbf{z}')]$ for density-density correlations, $\mathbf{C}^{\mathbf{xy}}_{\mathbf{J}\rho}(t) = \hat{\mathcal{I}}^{t,u}_{\mathbf{xy}}[\Xi^{\mathbf{zz}'}_2 - 2\mathbf{j}_{\rm s}(\mathbf{z}) p_{\rm s}(\mathbf{z}')]$ for current-density correlations, and (see Ref. [90]) $C^{\mathbf{xy}}_{\mathbf{J}\cdot\mathbf{J}}(t) = \hat{\mathcal{I}}^{t,U}_{\mathbf{xy}}[\Xi^{\mathbf{zz}'}_3 - 2\mathbf{j}_{\rm s}(\mathbf{z}) \cdot \mathbf{j}_{\rm s}(\mathbf{z}')]$ for current-current correlations, where we defined

$$\begin{aligned}
\Xi^{\mathbf{zz}'}_1 &\equiv \langle 1 \rangle_{\mathbf{x}_{t_1}=\mathbf{z}}^{\mathbf{x}_{t_2}=\mathbf{z}'} + \langle 1 \rangle_{\mathbf{x}_{t_1}=\mathbf{z}'}^{\mathbf{x}_{t_2}=\mathbf{z}}, \\
\Xi^{\mathbf{zz}'}_2 &\equiv \frac{\langle \circ d\mathbf{x}_{t_1} \rangle_{\mathbf{x}_{t_1}=\mathbf{z}}^{\mathbf{x}_{t_2}=\mathbf{z}'}}{dt_1} + \frac{\langle \circ d\mathbf{x}_{t_2} \rangle_{\mathbf{x}_{t_1}=\mathbf{z}'}^{\mathbf{x}_{t_2}=\mathbf{z}}}{dt_2}, \\
\Xi^{\mathbf{zz}'}_3 &\equiv \frac{\langle \circ d\mathbf{x}_{t_1} \cdot \circ d\mathbf{x}_{t_2} \rangle_{\mathbf{x}_{t_1}=\mathbf{z}}^{\mathbf{x}_{t_2}=\mathbf{z}'}}{dt_1 dt_2} + \frac{\langle \circ d\mathbf{x}_{t_1} \cdot \circ d\mathbf{x}_{t_2} \rangle_{\mathbf{x}_{t_1}=\mathbf{z}'}^{\mathbf{x}_{t_2}=\mathbf{z}}}{dt_1 dt_2}.
\end{aligned} \qquad (4)$$

Equations (3) and (4) tie $C^{\mathbf{xy}}_{AB}$ to properties of pinned paths, weighted by $U^h_{\mathbf{x}}(\mathbf{z})$, $U^h_{\mathbf{y}}(\mathbf{z}')$ and integrated over space and times $0 \leq t_1 \leq t_2 \leq t$. In contrast to the somewhat better understood density-density covariance [23,29,91], current-density and current-current covariances involve (scalar products of) more subtle Stratonovich increments along pinned trajectories, explained graphically in Fig. 2 and further investigated in the following.

Correlations and fluctuations from two-point densities.—To obtain quantitative results, we evaluate the averages $\langle \cdot \rangle_{\mathbf{x}_{t_1}=\mathbf{z}}^{\mathbf{x}_{t_2}=\mathbf{z}'}$ in terms of two-point functions $P_{\mathbf{z}}(\mathbf{z}', t_2 - t_1) \equiv G(\mathbf{z}', t_2 - t_1 | \mathbf{z}) p_{\rm s}(\mathbf{z})$. For density-density correlations $C^{\mathbf{xy}}_{\rho\rho}$ the result is readily obtained from Eq. (4) using $\langle 1 \rangle_{\mathbf{x}_{t_1}=\mathbf{z}}^{\mathbf{x}_{t_2}=\mathbf{z}'} = P_{\mathbf{z}}(\mathbf{z}', t_2 - t_1)$. Conversely, Stratonovich increments are difficult to understand and hard to evaluate, particularly initial-point increments $\circ d\mathbf{x}_{t_1}$ because they are correlated with future events.

To gain intuition we examine a two-dimensional shear flow $\mathbf{F}_{\rm sh}(\mathbf{x}) = 2x\hat{\mathbf{y}}$ shown in Fig. 2, depicting initial-, $\circ d\mathbf{x}_{t_1}$, and end-point, $\circ d\mathbf{x}_{t_2}$, increments along forward [Fig. 2(a)] and time-reversed [Fig. 2(b)] pinned trajectories between times $t_1 < t_2$ and their ensemble averages [Figs. 2(d) and 2(e)]. In the companion extended paper [40] we show that $\langle \circ d\mathbf{x}_{t_2} \rangle^{\mathbf{x}_{t_2}=\mathbf{z}'}_{\mathbf{x}_{t_1}=\mathbf{z}} = \hat{\mathbf{j}}_{\mathbf{z}'} P_{\mathbf{z}}(\mathbf{z}', t_2) dt_2$, i.e., mean displacements are given by the Fokker-Planck current as expected. Moreover, when detailed balance holds, time-reversal symmetry implies $\mathbb{P}(\circ d\mathbf{x}_{t_1}|^{\mathbf{x}_{t_2}=\mathbf{z}'}_{\mathbf{x}_{t_1}=\mathbf{z}}) = \mathbb{P}(-\circ d\mathbf{x}_{t_2}|^{\mathbf{x}_{t_2}=\mathbf{z}}_{\mathbf{x}_{t_1}=\mathbf{z}'})$, whereas under broken detailed balance, e.g., due to the shear flow in Fig. 2, this ceases to hold. We may, however, employ a generalized time-reversal symmetry—the dual-reversal symmetry (see Refs. [27,40,92,93])—implying $\mathbb{P}(\circ d\mathbf{x}_{t_1}|^{\mathbf{x}_{t_2}=\mathbf{z}'}_{\mathbf{x}_{t_1}=\mathbf{z}}) = \mathbb{P}(-\circ d\mathbf{x}^{-\mathbf{j}_{\rm s}}_{t_2}|^{\mathbf{x}_{t_2}=\mathbf{z}}_{\mathbf{x}_{t_1}=\mathbf{z}'})$ connecting ensembles with currents $\mathbf{j}_{\rm s}$ and $-\mathbf{j}_{\rm s}$ [see Figs. 2(c), 2(f), and 2(g)]. Via this generalized time-reversal symmetry we circumvent the correlation of $\circ d\mathbf{x}_{t_1}$ with the future. To materialize this we isolate the irreversible drift in $\hat{\mathbf{j}}_{\mathbf{x}} = p_{\rm s}(\mathbf{x})^{-1}\mathbf{j}_{\rm s}(\mathbf{x}) - p_{\rm s}(\mathbf{x})\mathbf{D}\nabla_{\mathbf{x}} p_{\rm s}(\mathbf{x})^{-1}$, and introduce the dual current operator $\hat{\mathbf{j}}^{\ddagger}_{\mathbf{x}} \equiv -\hat{\mathbf{j}}^{-\mathbf{j}_{\rm s}}_{\mathbf{x}} = p_{\rm s}(\mathbf{x})^{-1}\mathbf{j}_{\rm s}(\mathbf{x}) + p_{\rm s}(\mathbf{x})\mathbf{D}\nabla_{\mathbf{x}} p_{\rm s}(\mathbf{x})^{-1}$, rendering all terms in Eq. (4) [illustrated in Fig. 2(h)] tractable, and ultimately leading to our main result

$$\begin{aligned} \mathbf{C}^{\mathbf{xy}}_{\mathbf{J}_\rho}(t) &= \hat{\mathcal{I}}^{t,U}_{\mathbf{xy}}[\hat{\mathbf{j}}_{\mathbf{z}} P_{\mathbf{z}'}(\mathbf{z}, t') + \hat{\mathbf{j}}^{\ddagger}_{\mathbf{z}} P_{\mathbf{z}}(\mathbf{z}', t') - 2\mathbf{j}_{\rm s}(\mathbf{z}) p_{\rm s}(\mathbf{z}')], \\ C^{\mathbf{xy}}_{\mathbf{J}\cdot\mathbf{J}}(t) &= \frac{2{\rm Tr}\mathbf{D}}{t} \int d\mathbf{z} U^h_{\mathbf{x}}(\mathbf{z}) U^h_{\mathbf{y}}(\mathbf{z}) p_{\rm s}(\mathbf{z}) + \hat{\mathcal{I}}^{t,U}_{\mathbf{xy}}[\hat{\mathbf{j}}_{\mathbf{z}} \cdot \hat{\mathbf{j}}^{\ddagger}_{\mathbf{z}'} P_{\mathbf{z}'}(\mathbf{z}, t') + \hat{\mathbf{j}}_{\mathbf{z}'} \cdot \hat{\mathbf{j}}^{\ddagger}_{\mathbf{z}} P_{\mathbf{z}}(\mathbf{z}', t') - 2\mathbf{j}_{\rm s}(\mathbf{z}) \cdot \mathbf{j}_{\rm s}(\mathbf{z}')], \end{aligned} \tag{5}$$

where the first term in $C^{\mathbf{xy}}_{\mathbf{J}\cdot\mathbf{J}}(t)$ arises from $t_1 = t_2$ [40], and the operator $\hat{\mathcal{I}}^{t,U}_{\mathbf{xy}}$ simplifies $t^{-2}\int_0^t dt_1 \int_{t_1}^t dt_2 \to t^{-1}\int_0^t dt'(1 - t'/t)$ since Eq. (5) depends only on time differences $t' \equiv t_2 - t_1 \geq 0$. Notably, written in this simplified form Eq. (5) establishes Green-Kubo relations [94,95] connecting covariances $C^{\mathbf{xy}}_{AB}$ to time-integrals of generalized correlation functions.

Given the two-point function $P_{\mathbf{z}}(\mathbf{z}', t')$, Eq. (5) gives the correlation and fluctuations of observables defined in Eq. (1). In practice, $P_{\mathbf{z}}(\mathbf{z}', t')$ may not necessarily be available. However, the theoretical result Eq. (5) nevertheless allows us to draw several conclusions, in particular by considering special cases and limits. At equilibrium $\hat{\mathbf{j}}^{\ddagger}_{\mathbf{z}} = -\hat{\mathbf{j}}_{\mathbf{z}}$, implying $\mathbf{C}^{\mathbf{xy}}_{\mathbf{J}_\rho}(t) = 0$. A nonzero $\mathbf{C}^{\mathbf{xy}}_{\mathbf{J}_\rho}(t)$ at any time t is thus a conclusive signature of broken detailed balance. Moreover, at equilibrium $C^{\mathbf{xy}}_{\mathbf{J}\cdot\mathbf{J}}(t)$ does not vanish although $\langle \overline{\mathbf{J}^U_{\mathbf{x}}} \rangle_{\rm s} = 0$. When $\mathbf{j}_{\rm s} \neq \mathbf{0}$, ${\rm var}^{\mathbf{x}}_{\mathbf{J}}(t) \equiv C^{\mathbf{xx}}_{\mathbf{J}\cdot\mathbf{J}}(t)$ may display maxima where $P_{\rm s}(\mathbf{x})$ has none [see Figs. 3(a)–3(c)], and an oscillatory time dependence due to circulating currents [see Fig. 3(d)], both signaling nonequilibrium. For a more detailed discussion of Eq. (5), see Ref. [40].

Necessity of coarse graining.—Of particular interest is the dependence of fluctuations on the coarse-graining length scale h (see Figs. 1(f) and 3(c) and Ref. [40]). Importantly, the limits $h \to \infty$ and $h \to 0$ are generally accessible from Eq. (5) independent of the detailed dynamics (see Ref. [40]). The limit $h \to 0$ with $U^h_{\mathbf{x}}(\mathbf{z}) \to \delta(\mathbf{x} - \mathbf{z})$ corresponds to no coarse graining, i.e., the observables Eq. (1) are evaluated in a single point $\mathbf{z}$. In this limit, the

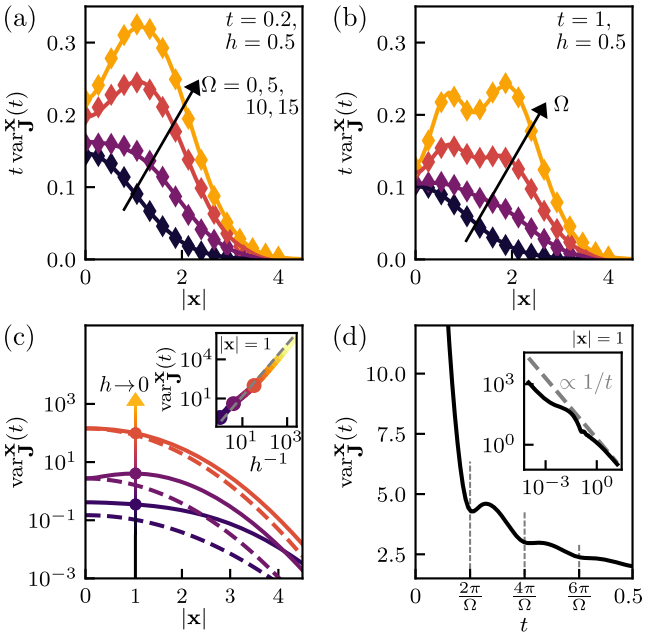

FIG. 3. $t{\rm var}^{\mathbf{x}}_{\mathbf{J}}$ as a function of the radius $|\mathbf{x}|$ in the harmonically confined rotational flow in Fig. 1(c) for increasing Ω with Gaussian $U^h_{\mathbf{x}}$ with width h at (a) $t = 0.2$ and (b) $t = 1$; lines depict Eq. (5) and symbols simulations [80]. (c) $t{\rm var}^{\mathbf{x}}_{\mathbf{J}}$ at $t = 1$ for $\Omega = 10$ (full lines) and equilibrium $\Omega = 0$ (dashed lines), for various h decreasing along the arrow. Inset: divergence of ${\rm var}^{\mathbf{x}}_{\mathbf{J}}$ as $h \to 0$ at $|\mathbf{x}| = 1$; the dashed line depicts Eq. (6). Note the logarithmic scales. (d) ${\rm var}^{\mathbf{x}}_{\mathbf{J}}$ as a function of t for very strong driving $\Omega = 50$; inset: (d) on logarithmic scales alongside the central-limit scaling $\propto t^{-1}$.

variance and covariance of $\overline{\rho^U_{\mathbf{x}}}$ and $\overline{\mathbf{J}^U_{\mathbf{x}}}$ for $d \geq 2$ and any t behave as [40]

$$\begin{aligned}
&\mathrm{var}^{\mathbf{x}}_{\rho}(t) \overset{h\to 0}{\simeq} \frac{k p_{\mathrm{s}}(\mathbf{x})}{t} \times \begin{cases} \frac{h^{2-d}}{d-2} & \text{for } d > 2, \\ -\ln h & \text{for } d = 2, \end{cases} \\
&\mathbf{C}^{\mathbf{xx}}_{\mathbf{J}\rho}(t) \overset{h\to 0}{\simeq} \mathbf{j}_{\mathrm{s}}(\mathbf{x}) \mathrm{var}^{\mathbf{x}}_{\rho}(t)/2p_{\mathrm{s}}(\mathbf{x}), \\
&\mathrm{var}^{\mathbf{x}}_{\mathbf{J}}(t) \overset{h\to 0}{=} \frac{k' p_{\mathrm{s}}(\mathbf{x})}{t}(d-1)h^{-d} + \mathcal{O}(t^{-1})\mathcal{O}(h^{1-d}), \quad (6)
\end{aligned}$$

where $\simeq$ denotes asymptotic equality, and k, k' are constants depending on $\mathbf{D}$ and $U_{\mathbf{x}}$ [40]. Therefore, taking $U^h_{\mathbf{x}}(\mathbf{z}) \overset{h\to 0}{\to} \delta(\mathbf{x}-\mathbf{z})$ as implicitly assumed in [23,42–50] we find for $d \geq 2$ that $\mathrm{var}^{\mathbf{x}}_{\rho,\mathbf{J}}(t)$, $\mathbf{C}^{\mathbf{xx}}_{\mathbf{J}\rho}(t)$ diverge for all t [see Fig. 3(c)]. Equation (6) also applies to Markov-jump processes defined on a grid with spacing $h \to 0$; for details and an example see Ref. [80]. The divergence can be understood intuitively [40], e.g., based on the following argument.

Note that the probability that point $\mathbf{z}$ is hit by the trajectory $(\mathbf{x}_\tau)_{0\leq\tau\leq t}$, i.e., that there is a $\tau \in [0,t]$ such that $\mathbf{x}_\tau = \mathbf{z}$, delicately depends on the spatial dimensionality d. This probability is positive for $d = 1$ but zero in higher-dimensional space. That is, $\mathbb{P}(\exists\, \tau \in (0,t] : \mathbf{x}_\tau = \mathbf{z}) = 0$ for diffusion in $d \geq 2$ [40,96]. Mean values remain finite in the limit $h \to 0$, namely $\langle \overline{\rho_{\mathbf{x}}}(t) \rangle_{\mathrm{s}} = p_{\mathrm{s}}(\mathbf{x})$ and $\langle \overline{\mathbf{J}_{\mathbf{x}}}(t) \rangle_{\mathrm{s}} = \mathbf{j}_{\mathrm{s}}(\mathbf{x})$ in agreement with existing literature [14,45–50,87]. Since the probability to hit the point $\mathbf{z}$ is approaching zero as $h \to 0$, this implies that the mean is precisely balanced by the infinite contribution of the delta function $U^h_{\mathbf{x}}(\mathbf{z}) \to \delta(\mathbf{x}-\mathbf{z})$, as in $\langle \delta(\mathbf{x}_\tau - \mathbf{x}) \rangle_{\mathrm{s}} = p_{\mathrm{s}}(\mathbf{x})$. Loosely speaking, here "$0 \times \infty$" is finite. One may therefore expect diverging second (and higher) moments when $h \to 0$ as this argument extends to "$0 \times \infty^2 = \infty$." The argument is not limited to overdamped motion but seems to extend to a larger class of stochastic dynamics, such as underdamped diffusion and experimental data on anomalous intracellular transport [97] shown in Fig. 9 of Ref. [40].

We hypothesize that not only the moments diverge, but that the density and current cannot even be consistently defined for $h = 0$. Moreover, the limits $h \to 0$ and $t \to \infty$ do *not* commute. This has important consequences for the central-limit regime, i.e., statistics on longest timescales (see Appendix B and [40]). Some coarse graining $h > 0$ is therefore necessary for mathematical consistency and anticipated central-limit properties.

Notably, for small windows Eq. (6) implies that fluctuations (unlike correlations) carry no information about steady-state currents $\mathbf{j}_{\mathrm{s}}(\mathbf{x})$ and thus violations of detailed balance and thermodynamic properties such as the system's dissipation. In this limit fluctuations reflect only Brownian, thermal currents that are invariant with respect to $\mathbf{j}_{\mathrm{s}}(\mathbf{x})$—systems with equal $p_{\mathrm{s}}(\mathbf{x})$ and $\mathbf{D}$ display identical fluctuations [see Eq. (6) and Fig. 3(c)]. Recall that the dissipation can be inferred from current fluctuations via the thermodynamic uncertainty relation [16,17,26]. We now see that only an intermediate coarse graining, such as the "optimum" in Fig. 1(f), allows us to infer dissipation from fluctuations. Moreover, spatial features of steady-state currents [see Fig. 3(c)] are only revealed with coarse graining. Some coarse graining $h > 0$ is thus necessary to infer thermodynamic properties. In addition, divergent fluctuations make it impossible to accurately infer densities and currents without coarse graining from experiments. Experiments also nominally have a finite spatial resolution. Thus, coarse graining is also experimentally necessary.

Conclusion.—Leveraging Itô calculus and generalized time-reversal symmetry we were able to provide elusive physical intuition about fluctuations and correlations of empirical densities and currents that are central to stochastic thermodynamics. We established the so far overlooked necessity for spatial coarse graining—it is required to ensure mathematically well defined observables and the validity of central-limit statements in dimensions $d \geq 2$, to improve the accuracy of inferring thermodynamic properties (e.g., dissipation) from fluctuations and to uncover salient features of nonequilibrium steady-state currents without inferring these individually [98–100], and is unavoidable in the analysis of experimental data with a finite resolution. Nonvanishing current-density correlations were shown to be a conclusive indicator of broken detailed balance, and may improve the accuracy of inferring invariant densities [101] and dissipation far from equilibrium [28]. Our results allow for generalizations to nonstationary initial conditions or nonergodic dynamics, which will be addressed in forthcoming publications.

Financial support from Studienstiftung des Deutschen Volkes (to C. D.) and the German Research Foundation (DFG) through the Emmy Noether Program GO 2762/1-2 (to A. G.) is gratefully acknowledged.

Appendix A: Density and current from sojourns.—In general the density and current functionals measure the ($U^h_{\mathbf{x}}$-weighted) time spent and displacement accumulated in the window $U^h_{\mathbf{x}}$ averaged over time. Specifically, when $U^h_{\mathbf{x}}$ is the indicator function, $U^h_{\mathbf{x}}(\mathbf{z}) = h^{-d}\mathbb{1}_{\Omega_{\mathbf{x}}}(\mathbf{z})$, of a region $\Omega_{\mathbf{x}}$ centered at $\mathbf{x}$ with volume h^d, we can write this illustratively in terms of the sojourns of the window as follows. Letting the times of entering and exiting said window be τ_i^- and τ_i^+, respectively, $t\overline{\rho^U_{\mathbf{x}}}(t)$ corresponds to the sum of sojourn times, $\tau_i^s = \tau_i^+ - \tau_i^-$, and $t\overline{\mathbf{J}^U_{\mathbf{x}}}(t)$ the sum of vectors $\delta\mathbf{x}_i^s$ between entrance $\mathbf{x}_{\tau_i^-}$ and exit $\mathbf{x}_{\tau_i^+}$ points, that is,

$$\begin{aligned}
t\overline{\rho^U_{\mathbf{x}}}(t) &= \frac{1}{h^d}\sum_{i\leq N_t}(\tau_i^+ - \tau_i^-) \equiv \frac{1}{h^d}\sum_{i\leq N_t}\tau_i^s, \\
t\overline{\mathbf{J}^U_{\mathbf{x}}}(t) &= \frac{1}{h^d}\sum_{i\leq N_t}(\mathbf{x}_{\tau_i^+} - \mathbf{x}_{\tau_i^-}) \equiv \frac{1}{h^d}\sum_{i\leq N_t}\delta\mathbf{x}_i^s, \quad \text{(A1)}
\end{aligned}$$

where N_t is the number of visits of the window. Note that N_t is almost surely either ∞ or 0, but the sum converges. The points $\mathbf{x}_0$ or $\mathbf{x}_t$ may lie within $U^h_{\mathbf{x}}$ for which we set $\mathbf{x}_{\tau_1^-} = \mathbf{x}_0$ and/or $\mathbf{x}_{\tau^+_{N_t}} \equiv \mathbf{x}_t$. As a result of correlations between $\mathbf{x}_{\tau_i^-}$ and τ_i^s as well as $\mathbf{x}_{\tau_i^+}$ and $\mathbf{x}_{\tau_{i+1}^-}$, $t\overline{\rho^U}$ and $t\overline{\mathbf{J}^U}$ are in general *not* renewal processes. A realization of $\mathbf{x}_\tau$ in Figs. 1(a) and 1(b) provides intuition about Eq. (A1).

Appendix B: Central-limit regime.—Since the observables defined in Eq. (1) involve time averages, their statistics on the longest timescales is expected to be governed by the central limit theorem. Indeed, for nonzero h or in spatial dimension $d = 1$ (in both cases we obtained finite variances) on timescales t that are very large compared to all timescales in the system, different parts of a trajectory [e.g., the sojourns in Fig. 1(a) and Eq. (A1)] become sufficiently uncorrelated such that the central limit theorem implies Gaussian statistics. However, the diverging variance for $h \to 0$ for $d \geq 2$ prevents Gaussian central-limit statistics on all timescales for the empirical density and current defined with a δ function (i.e., without coarse graining). Since the diverging part of the variance in Eq. (6) has the dominant central-limit scaling $\propto t^{-1}$, the asymptotic variance $\sigma_A^2 \overset{t\to\infty}{=} t\mathrm{var}^{\mathbf{x}}_A(t)$ [where $A_{\mathbf{x}}(t)$ denotes $\overline{\rho^U_{\mathbf{x}}}(t)$ or $\overline{\mathbf{J}^U_{\mathbf{x}}}(t)$] also diverges as $h \to 0$. This implies that taking $t \to \infty$ first and then $h \to 0$ also does *not* yield finite variances. Moreover, note that the longest timescale in the system becomes the recurrence time, which diverges as $h \to 0$. We hypothesize that a limiting distribution of $A_{\mathbf{x}}(t)$ only exists as a scaling limit where $h \to 0$ and $t \to \infty$ simultaneously in some d-dependent manner [40].

The central-limit regime is generally contained in the framework of large deviation theory [42,48,102]. Because of the divergent variance σ_A^2 and the resulting breakdown of Gaussian central-limit statistics, any large deviation principle for empirical densities and currents without coarse graining that predicts finite variances ceases to hold in $d \geq 2$.

*agodec@mpinat.mpg.de

[1] J. Gladrow, N. Fakhri, F. C. MacKintosh, C. F. Schmidt, and C. P. Broedersz, Phys. Rev. Lett. **116**, 248301 (2016).
[2] F. S. Gnesotto, F. Mura, J. Gladrow, and C. P. Broedersz, Rep. Prog. Phys. **81**, 066601 (2018).
[3] F. Ritort, J. Phys. Condens. Matter **18**, R531 (2006).
[4] W. J. Greenleaf, M. T. Woodside, and S. M. Block, Annu. Rev. Biophys. Biomol. Struct. **36**, 171 (2007).
[5] J. R. Moffitt, Y. R. Chemla, S. B. Smith, and C. Bustamante, Annu. Rev. Biochem. **77**, 205 (2008).
[6] S. Vaikuntanathan and C. Jarzynski, Europhys. Lett. **87**, 60005 (2009).
[7] C. Maes, K. Netočný, and B. Wynants, Phys. Rev. Lett. **107**, 010601 (2011).
[8] H. Qian, J. Math. Phys. (N.Y.) **54**, 053302 (2013).
[9] C. Maes, Phys. Rev. Lett. **119**, 160601 (2017).
[10] N. Shiraishi and K. Saito, Phys. Rev. Lett. **123**, 110603 (2019).
[11] A. Lapolla and A. Godec, Phys. Rev. Lett. **125**, 110602 (2020).
[12] T. Koyuk and U. Seifert, Phys. Rev. Lett. **125**, 260604 (2020).
[13] D.-Q. Jiang, M. Qian, and M.-P. Qian, *Mathematical Theory of Nonequilibrium Steady States* (Springer, Berlin, Heidelberg, 2004).
[14] C. Maes, K. Netočný, and B. Wynants, Physica (Amsterdam) **387A**, 2675 (2008).
[15] C. Maes and K. Netočný, Europhys. Lett. **82**, 30003 (2008).
[16] T. R. Gingrich, J. M. Horowitz, N. Perunov, and J. L. England, Phys. Rev. Lett. **116**, 120601 (2016).
[17] A. C. Barato and U. Seifert, Phys. Rev. Lett. **114**, 158101 (2015).
[18] A. Dechant and S.-i. Sasa, J. Stat. Mech. (2018) 063209.
[19] U. Seifert and T. Speck, Europhys. Lett. **89**, 10007 (2010).
[20] E. N. M. Cirillo, M. Colangeli, O. Richardson, and L. Rondoni, Phys. Rev. E **103**, 032119 (2021).
[21] D. J. Evans, S. R. Williams, D. J. Searles, and L. Rondoni, J. Stat. Phys. **164**, 842 (2016).
[22] S. Burov, J.-H. Jeon, R. Metzler, and E. Barkai, Phys. Chem. Chem. Phys. **13**, 1800 (2011).
[23] A. Lapolla, D. Hartich, and A. Godec, Phys. Rev. Research **2**, 043084 (2020).
[24] H. Qian, Phys. Rev. E **64**, 022101 (2001).
[25] J. M. Horowitz and T. R. Gingrich, Nat. Phys. **16**, 15 (2020).
[26] T. R. Gingrich, G. M. Rotskoff, and J. M. Horowitz, J. Phys. A **50**, 184004 (2017).
[27] A. Dechant and S.-i. Sasa, Phys. Rev. Research **3**, L042012 (2021).
[28] A. Dechant and S.-i. Sasa, Phys. Rev. X **11**, 041061 (2021).
[29] M. Kac, Trans. Am. Math. Soc. **65**, 1 (1949).
[30] D. A. Darling and M. Kac, Trans. Am. Math. Soc. **84**, 444 (1957).
[31] E. Aghion, D. A. Kessler, and E. Barkai, Phys. Rev. Lett. **122**, 010601 (2019).
[32] S. Carmi and E. Barkai, Phys. Rev. E **84**, 061104 (2011).
[33] S. N. Majumdar and A. Comtet, Phys. Rev. Lett. **89**, 060601 (2002).
[34] S. N. Majumdar and D. S. Dean, Phys. Rev. E **66**, 041102 (2002).
[35] S. N. Majumdar, Curr. Sci. **89**, 2075 (2005).
[36] A. J. Bray, S. N. Majumdar, and G. Schehr, Adv. Phys. **62**, 225 (2013).
[37] G. Bel and E. Barkai, Phys. Rev. Lett. **94**, 240602 (2005).
[38] C. Battle, C. P. Broedersz, N. Fakhri, V. F. Geyer, J. Howard, C. F. Schmidt, and F. C. MacKintosh, Science **352**, 604 (2016).
[39] J. Li, J. M. Horowitz, T. R. Gingrich, and N. Fakhri, Nat. Commun. **10**, 1666 (2019).
[40] C. Dieball and A. Godec, companion paper, Phys. Rev. Res. **4**, 033243 (2022).
[41] A. Dechant, J. Phys. A **52**, 035001 (2019).

[42] H. Touchette, Phys. Rep. **478**, 1 (2009).
[43] S. Kusuoka, K. Kuwada, and Y. Tamura, Probab. Theory Relat. Fields **147**, 649 (2010).
[44] R. Chetrite and H. Touchette, Phys. Rev. Lett. **111**, 120601 (2013).
[45] R. Chetrite and H. Touchette, Ann. Henri Poincaré **16**, 2005 (2014).
[46] A. C. Barato and R. Chetrite, J. Stat. Phys. **160**, 1154 (2015).
[47] J. Hoppenau, D. Nickelsen, and A. Engel, New J. Phys. **18**, 083010 (2016).
[48] H. Touchette, Physica (Amsterdam) **504A**, 5 (2018).
[49] E. Mallmin, J. du Buisson, and H. Touchette, J. Phys. A **54**, 295001 (2021).
[50] C. Monthus, J. Stat. Mech. (2021) 063211.
[51] É. Roldán and J. M. R. Parrondo, Phys. Rev. Lett. **105**, 150607 (2010).
[52] É. Fodor, C. Nardini, M. E. Cates, J. Tailleur, P. Visco, and F. van Wijland, Phys. Rev. Lett. **117**, 038103 (2016).
[53] J. Gladrow, M. Ribezzi-Crivellari, F. Ritort, and U. F. Keyser, Nat. Commun. **10**, 55 (2019).
[54] A. M. Berezhkovskii and D. E. Makarov, J. Phys. Chem. Lett. **11**, 1682 (2020).
[55] D. S. Seara, B. B. Machta, and M. P. Murrell, Nat. Commun. **12**, 392 (2021).
[56] L. F. Cugliandolo, D. S. Dean, and J. Kurchan, Phys. Rev. Lett. **79**, 2168 (1997).
[57] D. Mizuno, C. Tardin, C. F. Schmidt, and F. C. MacKintosh, Science **315**, 370 (2007).
[58] U. Seifert, Rep. Prog. Phys. **75**, 126001 (2012).
[59] S. Pigolotti, I. Neri, É. Roldán, and F. Jülicher, Phys. Rev. Lett. **119**, 140604 (2017).
[60] U. Seifert, Physica (Amsterdam) **504A**, 176 (2018).
[61] S. Otsubo, S. Ito, A. Dechant, and T. Sagawa, Phys. Rev. E **101**, 062106 (2020).
[62] S. K. Manikandan, D. Gupta, and S. Krishnamurthy, Phys. Rev. Lett. **124**, 120603 (2020).
[63] J. L. Lebowitz and H. Spohn, J. Stat. Phys. **95**, 333 (1999).
[64] H. Qian, S. Saffarian, and E. L. Elson, Proc. Natl. Acad. Sci. U.S.A. **99**, 10376 (2002).
[65] S. Pilgram, A. N. Jordan, E. V. Sukhorukov, and M. Büttiker, Phys. Rev. Lett. **90**, 206801 (2003).
[66] T. Bodineau and B. Derrida, Phys. Rev. Lett. **92**, 180601 (2004).
[67] D. Andrieux and P. Gaspard, J. Stat. Phys. **127**, 107 (2007).
[68] L. Bertini, A. De Sole, D. Gabrielli, G. Jona-Lasinio, and C. Landim, Phys. Rev. Lett. **94**, 030601 (2005).
[69] R. K. P. Zia and B. Schmittmann, J. Stat. Mech. (2007) P07012.
[70] M. Baiesi, C. Maes, and K. Netočný, J. Stat. Phys. **135**, 57 (2009).
[71] P. Pietzonka, A. C. Barato, and U. Seifert, Phys. Rev. E **93**, 052145 (2016).
[72] T. R. Gingrich and J. M. Horowitz, Phys. Rev. Lett. **119**, 170601 (2017).
[73] S. C. Kapfer and W. Krauth, Phys. Rev. Lett. **119**, 240603 (2017).
[74] K. Macieszczak, K. Brandner, and J. P. Garrahan, Phys. Rev. Lett. **121**, 130601 (2018).
[75] M. Kaiser, R. L. Jack, and J. Zimmer, J. Stat. Phys. **170**, 1019 (2018).
[76] A. C. Barato, R. Chetrite, A. Faggionato, and D. Gabrielli, New J. Phys. **20**, 103023 (2018).
[77] S. Marcantoni, C. Pérez-Espigares, and J. P. Garrahan, Phys. Rev. E **101**, 062142 (2020).
[78] D. Hartich and A. Godec, Phys. Rev. X **11**, 041047 (2021).
[79] E. Suárez, R. P. Wiewiora, C. Wehmeyer, F. Noé, J. D. Chodera, and D. M. Zuckerman, J. Chem. Theory Comput. **17**, 3119 (2021).
[80] See Supplemental Material at http://link.aps.org/supplemental/10.1103/PhysRevLett.129.140601 for further details and auxiliary results, as well as Refs. [26,79,81–85].
[81] C. W. Gardiner, *Handbook of Stochastic Methods for Physics, Chemistry, and the Natural Sciences* (Springer-Verlag, Berlin, New York, 1985).
[82] A. Lapolla and A. Godec, Phys. Rev. Research **3**, L022018 (2021).
[83] V. Holubec, K. Kroy, and S. Steffenoni, Phys. Rev. E **99**, 032117 (2019).
[84] A. Meurer *et al.*, PeerJ Comput. Sci. **3**, e103 (2017).
[85] C. Dieball and A. Godec, arXiv:2206.04034.
[86] F. Flandoli, M. Gubinelli, M. Giaquinta, and V. M. Tortorelli, Stoch. Proc. Appl. **115**, 1583 (2005).
[87] V. Y. Chernyak, M. Chertkov, S. V. Malinin, and R. Teodorescu, J. Stat. Phys. **137**, 109 (2009).
[88] L. Bertini, A. De Sole, D. Gabrielli, G. Jona-Lasinio, and C. Landim, Rev. Mod. Phys. **87**, 593 (2015).
[89] G. A. Pavliotis, *Stochastic Processes and Applications* (Springer, New York, 2014).
[90] Fluctuations and correlations of $\overline{\mathbf{J}_{\mathbf{x}}^{U}}(t)$ are characterized by the $d \times d$ covariance matrix with elements $[\mathsf{C}_{\mathbf{JJ}}^{\mathbf{xy}}(t)]_{ik} = C_{\mathrm{J}_i\mathrm{J}_k}^{\mathbf{xy}}(t)$. We focus on the scalar case $C_{\mathbf{J}\cdot\mathbf{J}}^{\mathbf{xy}}(t) \equiv \mathrm{Tr}\mathsf{C}_{\mathbf{JJ}}^{\mathbf{xy}}(t)$. See [85] for the full covariance matrix.
[91] A. Lapolla and A. Godec, New J. Phys. **20**, 113021 (2018).
[92] S.-i. Sasa, J. Stat. Mech. 2014, P01004 (2014).
[93] T. Hatano and S.-i. Sasa, Phys. Rev. Lett. **86**, 3463 (2001).
[94] M. S. Green, J. Chem. Phys. **22**, 398 (1954).
[95] R. Kubo, J. Phys. Soc. Jpn. **12**, 570 (1957).
[96] R. Durrett, *Stochastic Calculus: A Practical Introduction*, 1st ed. (CRC Press, Boca Raton, 1996).
[97] A. Sabri, X. Xu, D. Krapf, and M. Weiss, Phys. Rev. Lett. **125**, 058101 (2020).
[98] A. Frishman and P. Ronceray, Phys. Rev. X **10**, 021009 (2020).
[99] D. B. Brückner, P. Ronceray, and C. P. Broedersz, Phys. Rev. Lett. **125**, 058103 (2020).
[100] F. Ferretti, V. Chardès, T. Mora, A. M. Walczak, and I. Giardina, Phys. Rev. X **10**, 031018 (2020).
[101] D. Hartich and U. Seifert, Phys. Rev. E **94**, 042416 (2016).
[102] A. Dembo and O. Zeitouni, *Large Deviations Techniques and Applications* (Springer, Berlin, Heidelberg, 2010).